Moisture-responsive root-branching pathways identified in diverse maize breeding germplasm

Johannes D. Scharwies, Taylor Clarke, Zihao Zheng, Andrea Dinneny, Siri Birkeland, Margaretha A. Veltman, Craig J. Sturrock, Jason Banda, Héctor H. Torres-Martínez, Willian G. Viana, Ria Khare, Joseph Kieber, Bipin K. Pandey, Malcolm Bennett, Patrick S. Schnable, José R. Dinneny

DOI:
https://www.science.org/doi/10.1126/science.ads5999

PLANT SCIENCE

Moisture-responsive root-branching pathways identified in diverse maize breeding germplasm

Johannes D. Scharwies[1]*, Taylor Clarke[1], Zihao Zheng[2]†, Andrea Dinneny[1], Siri Birkeland[3]‡, Margaretha A. Veltman[4,5]§, Craig J. Sturrock[6], Jason Banda[6], Héctor H. Torres-Martínez[1], Willian G. Viana[1], Ria Khare[7], Joseph Kieber[7], Bipin K. Pandey[6], Malcolm Bennett[6], Patrick S. Schnable[2], José R. Dinneny[1,8]*

Plants grow complex root systems to extract unevenly distributed resources from soils. Spatial differences in soil moisture are perceived by root tips, leading to the patterning of new root branches toward available water in a process called hydropatterning. Little is known about hydropatterning behavior and its genetic basis in crop plants. Here, we developed an assay to measure hydropatterning in maize and revealed substantial differences between tropical/subtropical and temperate maize breeding germplasm that likely resulted from divergent selection. Genetic analysis of hydropatterning confirmed the regulatory role of auxin and revealed that the gaseous hormone ethylene locally inhibits root branching from air-exposed tissues. Our results demonstrate how distinct signaling pathways translate spatial patterns of water availability to developmental programs that determine root architecture.

Climate change is predicted to increase the duration and severity of droughts (*1*). This will threaten crop production, which depends heavily on water. Plant water uptake is facilitated by an intricate network of roots. Breeding plants with improved root access to water is a potential method to make crops resilient to climate change (*2*). Root networks are established by branching of the primary root axis. The development of lateral root branches is highly responsive to the spatiotemporal distribution of resources such as water and nutrients in soils (*3*, *4*). Plants sense micrometer-scale heterogeneity in water availability at their root tips, with spatial differences along the root tip circumference determining the patterning of lateral roots through hydropatterning (*5*, *6*) (Fig. 1A). This response may allow plants to capture water more efficiently while minimizing the metabolic cost of root growth in dry soil (*7*). Understanding the extent of phenotypic variation for this trait within breeding populations and determining its genetic basis may facilitate crop improvement. Furthermore, understanding the mechanistic basis of hydropatterning will illuminate how heterogeneity in moisture is sensed by organisms to enact an adaptive response.

Hydropatterning in domesticated maize

Here, we investigated hydropatterning in the cereal crop species maize (*Zea mays*), which constitutes a major source of calories worldwide. To capture the phenotypic diversity of hydropatterning, we developed an assay using germination paper to create a controlled gradient of water availability across the circumference of the growing primary root (Fig. 1B and fig. S1). Simultaneous characterization of a diverse set of 250 maize inbred lines (data S1) from the Goodman-Buckler association panel allowed us to cover most of the genetic diversity present in current public sector breeding programs (*8*).

For all tested maize inbred lines, we observed that primary roots preferentially formed lateral roots on the side touching the water-saturated germination paper (the contact side), which is consistent with the inductive effect of water availability previously observed in the maize reference inbred B73 and in other species (*5*) (Fig. 1C and data S2). Nevertheless, a substantial proportion of all surveyed maize inbred lines developed air-side lateral roots as well, resulting in an observed phenotypic range of 0 to 39% air-side lateral roots across all 250 inbred lines (Fig. 1D). This suggests that a larger portion of maize inbred lines exhibit weakened hydropatterning (i.e., more air-side lateral roots) than previously indicated (*9*). Additionally, in a set of 20 maize inbred lines with diverse hydropatterning responses, we observed that hydropatterning in primary roots was significantly correlated to hydropatterning in crown roots, which make up the bulk of mature maize root systems (fig. S2, A to C, and data S3). Our results highlight the substantial variation of hydropatterning across maize root types, allowing this trait to be used for understanding how quantitative genetic variation contributes to overall root architecture.

In the B73 maize inbred line, lateral root founder cells initiate primordium development ~12 mm from the root tip (*10*). Prior research using B73 found that moisture availability cues, which determine the patterning of lateral roots, are perceived closer to the root tip, specifically within the first 5 to 6 mm (*9*). This suggests that moisture cues act on lateral root development at the founder cell patterning stage rather than at later developmental stages. Comparing lateral root patterning in several strong (<5% air-side lateral roots) and weak (>20% air-side lateral roots) hydropatterning inbred lines, we found that pre-emerged lateral root primordia and post-emergence lateral roots exhibited the same bias in distribution between the contact sides and the air sides, corresponding to the hydropatterning strength of each inbred line (fig. S2, D and E). Our observations provide further evidence that hydropatterning primarily acts at the lateral root founder cell patterning stage.

We next investigated how the observed variation in hydropatterning correlates with root architecture in soil conditions. In nature, large air spaces in the soil matrix called macropores are commonly created by prior root growth or burrowing invertebrate activity, such as by earthworms. We tested how lateral roots were patterned when primary roots were grown through artificial macropores. Strong hydropatterning inbred lines initiated their lateral roots preferentially toward the side of the root in contact with soil, as observed by microscale x-ray computed tomography (Fig. 1E). By contrast, weak hydropatterning inbred lines displayed a reduced bias, with more lateral roots growing into the air-filled macropore. Quantification across multiple strong and weak hydropatterning inbred lines found that they made similar percentages of air-side lateral roots in the soil macropore and our hydropatterning assay (fig. S2, F to H). These results demonstrate that our hydropatterning assay generates reproducible phenotypes that translate to soil conditions.

To explore how variation in hydropatterning relates to other phenotypic traits of field-grown maize plants, we performed a correlation analysis with 64 compiled trait sets measured from field-grown plants (*11*). We found that both air-side lateral root density and the percentage of air-side lateral roots correlated significantly with root crown depth and the number of nodes with brace roots (fig. S3, A to C, and data S4). Weaker hydropatterning inbred lines generally exhibited more shallow root systems with fewer brace roots according to data collected in two studies from Iowa (fig. S3, D to F) (*12*, *13*). This suggests that more efficient placement of root branches toward water may improve the ability of root systems to attain greater depths, possibly due to the metabolic

[1]Department of Biology, Stanford University, Stanford, CA, USA. [2]Department of Agronomy, Iowa State University, Ames, IA, USA. [3]Faculty of Chemistry, Biotechnology and Food Science, Norwegian University of Life Sciences, Ås, Norway. [4]Natural History Museum, University of Oslo, Oslo, Norway. [5]Naturalis Biodiversity Center, CR Leiden, Netherlands. [6]Plant and Crop Sciences, School of Biosciences, University of Nottingham, Sutton Bonington, UK. [7]Department of Biology, University of North Carolina, Chapel Hill, NC, USA. [8]Howard Hughes Medical Institute, Stanford University, Stanford, CA, USA.
***Corresponding author. Email: joscha@stanford.edu (J.D.S.); dinneny@stanford.edu (J.R.D.)**
†Present address: Vegetable & Flower Seeds Development, Syngenta Crop Protection LLC, Greensboro, NC, USA.
‡Present address: Natural History Museum, University of Oslo, Oslo, Norway.
§Present address: Institut de Recherche pour le Développement, Montpellier, France.

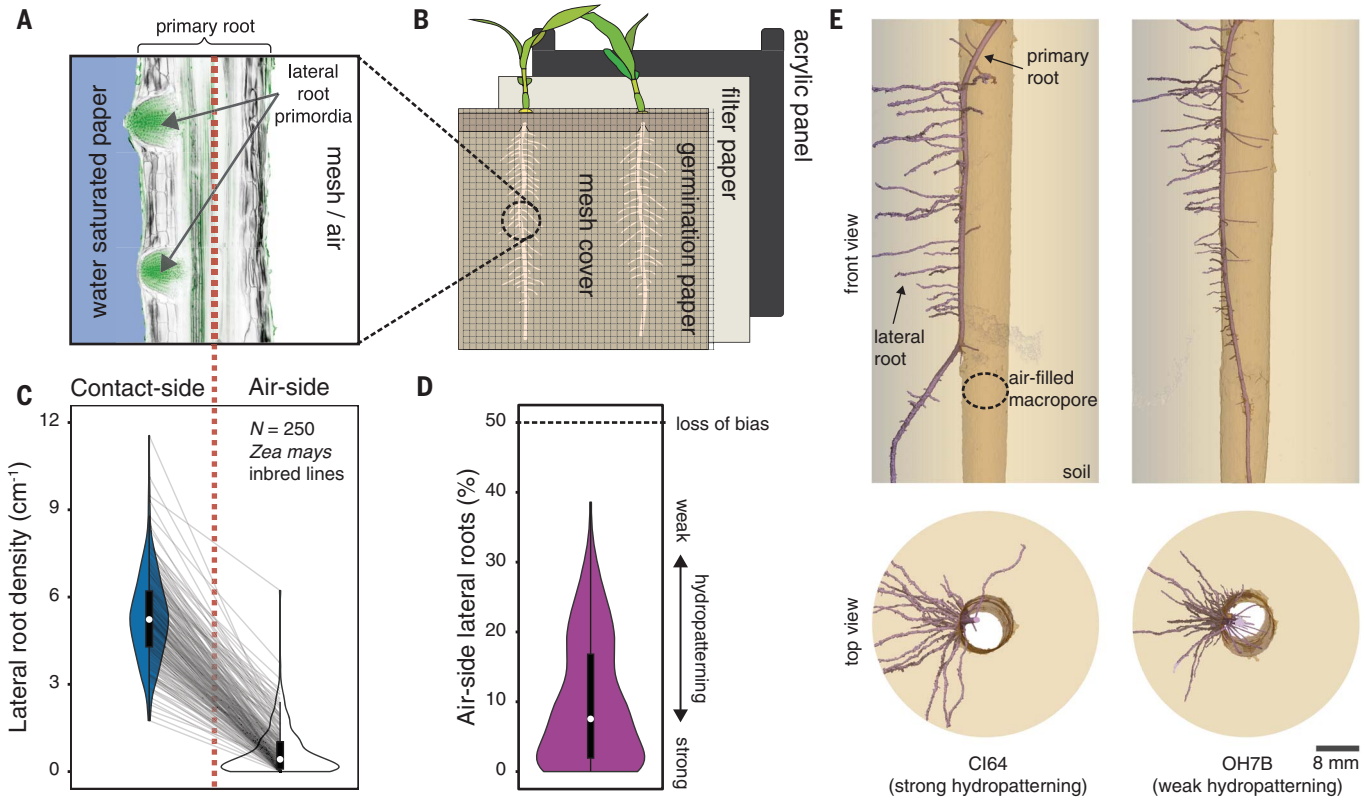

Fig. 1. Hydropatterning responses revealed in public sector breeding lines of maize. (**A** and **B**) Schematic of the hydropatterning response (A) in our custom-built hydropatterning assay (B). Primary roots of maize seedlings were grown in a vertical position along moist paper while being prevented from growing off the paper by a mesh cover. Lateral root primordia were preferentially induced toward the water-saturated paper (contact side) and suppressed on the air-exposed side (air side). Shown is a longitudinal cross section of maize root (B73 inbred) stained with calcofluor white (gray) and SYBR green (green) which stain cell walls and cell nuclei, respectively. The contact and air sides are separated by a dashed red line. (**C** and **D**) Distribution of contact-side (blue) and air-side (white) lateral root densities from 250 maize inbred lines characterized using the hydropatterning assay (C) and calculated percentage of air-side lateral roots (purple) (D). Each inbred line is represented by its median value (n = 1 to 3 seedlings per inbred line) (data S2). Gray lines connect corresponding inbred lines. Population median is shown as white circles. (**E**) Three-dimensionally rendered x-ray computed tomography images, viewed from the front and the top, showing lateral root patterning on primary roots of strong (CI64) and weak (OH7B) hydropatterning inbred lines grown through an air-filled macropore in soil.

savings achieved by limiting branching in dry soil (*14*). No significant correlations were observed with contact-side lateral root density, suggesting that this trait has less relevance to the in-field root architecture traits measured.

Variation and selection of hydropatterning across maize breeding subpopulations

We reassessed population structure and assigned subpopulations for all phenotyped inbred lines that had matching whole-genome sequencing data available (n = 231). Inbred lines with <80% subpopulation identity were assigned to a mixed group (*8*) (Fig. 2A and data S5). Although variation in contact-side lateral root density was uniform across all subpopulations, inbred lines with higher air-side lateral root density and a higher percentage of air-side lateral roots were predominantly associated with the non–stiff-stalk mixed groups (Fig. 2, B to D). This led to significantly weaker hydropatterning for the large temperate non–stiff-stalk group compared with the large tropical/subtropical group or the smaller temperate–stiff-stalk group (Fig. 2E and fig. S4A).

To test whether this divergence in hydropatterning was best explained by neutral evolution or selection, we compared quantitative genetic differentiation with regard to contact-side or air-side lateral root density (Q_{ST}) to the population genetic differentiation due to genetic structure (F_{ST}). We found that Q_{ST} and F_{ST} distributions overlapped for contact-side lateral root density, which suggests that genetic differentiation for this trait occurred through neutral evolution. Conversely, Q_{ST} was significantly in excess of F_{ST} for air-side lateral root density, as well as the percentage of air-side lateral roots, indicating divergence through differential selection for these hydropatterning traits (Fig. 2F, fig. S4B, and data S6). Pairwise comparisons between subpopulations showed the largest $Q_{ST} - F_{ST}$ differences between the non–stiff-stalk and tropical/subtropical groups, suggesting that divergence in selective pressures for hydropatterning occurred predominantly after the split between tropical/subtropical and temperate germplasm (Fig. 2G, fig. S4C, and data S6). Stronger hydropatterning in the tropical/subtropical subpopulations may have resulted from selection for drought tolerance, among other abiotic stress factors, during breeding (*15*, *16*). By contrast, weakened hydropatterning in the temperate non–stiff-stalk subpopulation could be the result of relaxation in selection pressures on efficient water uptake in temperate environments. However, linkage between hydropatterning and other traits could have contributed to differences in hydropatterning between subpopulations. Pronounced $Q_{ST} > F_{ST}$ differences for air-side lateral root density and contrasting observations for contact-side lateral root density support our hypothesis, but inbreeding may inflate Q_{ST} estimates (*17*).

Genetic architecture of hydropatterning in domesticated maize

Previous work in *Arabidopsis* (*Arabidopsis thaliana*) has shown that the auxin-signaling

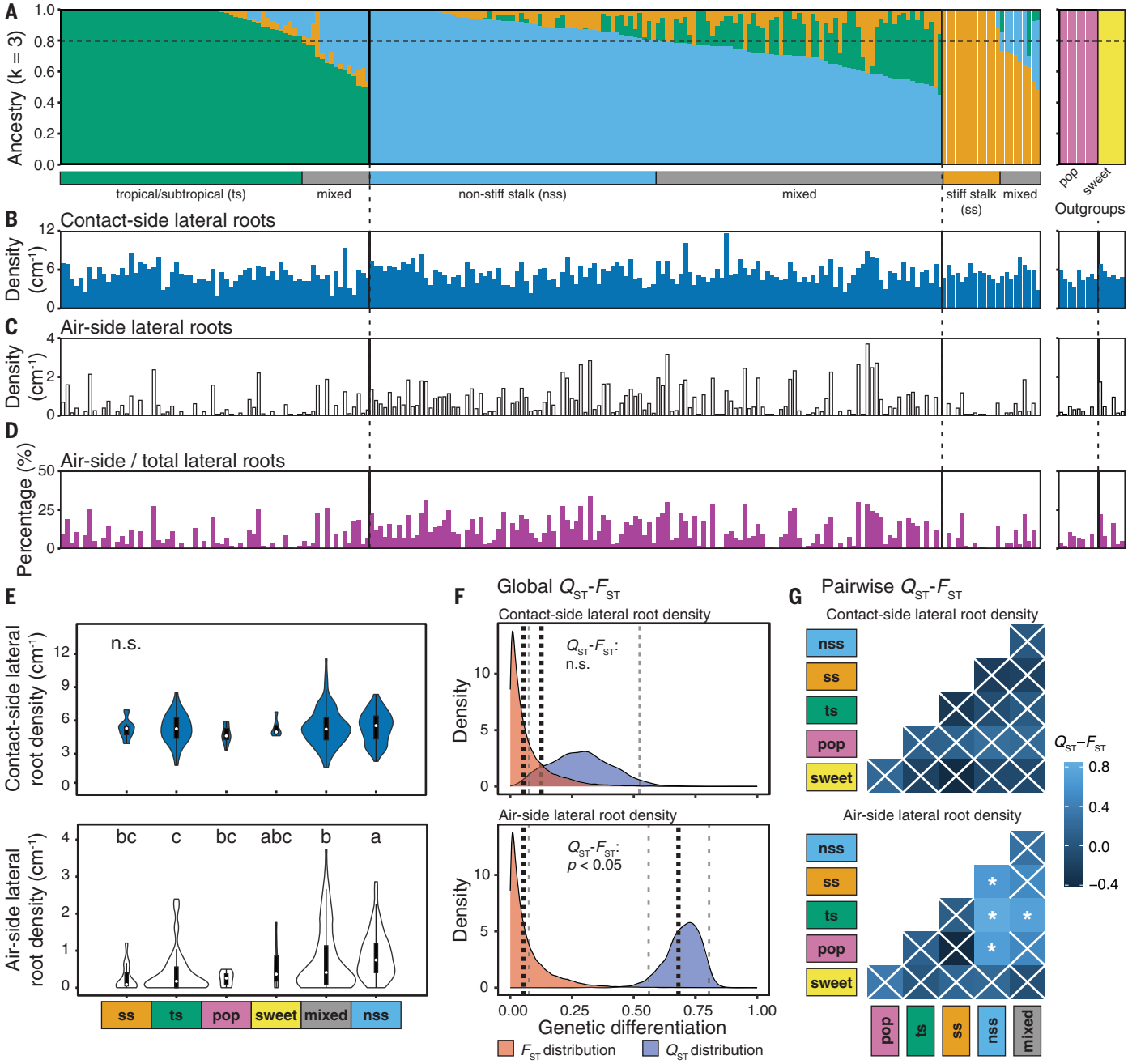

Fig. 2. Differences in hydropatterning across breeding subpopulations may have been caused by divergent selection. (**A** to **D**) Population structure and hydropatterning traits of 231 maize inbred lines (19 inbred lines from original population of N = 250 were excluded due to missing genotypic data). (A) Ancestry components and subpopulation assignments. Inbred lines <80% group identity (dashed line) is "mixed." Popcorn (pop) and sweet corn (sweet) groups were defined a priori. (B to D) Phenotypic data of contact-side (B) and air-side (C) lateral root density and percentage air-side lateral roots (D) are shown as the median value for each inbred line (n = 1 to 3 seedlings per inbred line) (data S2). (**E**) Subpopulation comparisons of contact-side (top) and air-side (bottom) lateral root density. Violin plot area was adjusted for the number of inbred lines/subpopulation. Letters denote significant differences between subpopulations ($P \leq 0.05$, Kruskal-Wallis and Dunn's post hoc tests); n.s., no significant differences. (**F**) Population-wide comparison of F_{ST} (fixation index) and Q_{ST} (genetic differentiation regarding a quantitative trait) distributions for contact-side (top) and air-side (bottom) lateral root density. Black dotted lines indicate means; gray dashed lines indicate 95% confidence intervals. (**G**) Subpopulation pairwise $Q_{ST} - F_{ST}$ comparisons. Asterisks denote significant differences between Q_{ST} and F_{ST} (*$P \leq 0.05$, Benjamini and Hochberg adjusted). White crosses, not significant. Number of inbred lines in each subpopulation across all panels: n_{ts} = 53, n_{nss} = 63, n_{ss} = 14, n_{mixed} = 88, n_{pop} = 9, and n_{sweet} = 6.

pathway promotes branching on the contact side of roots during hydropatterning. Mutants that disrupt auxin biosynthesis and polar transport are known to weaken hydropatterning (*5*). Similar to *Arabidopsis*, we found in maize that auxin accumulates preferentially on the contact side of hydropatterning roots, which creates a bias for lateral root induction (fig. S5). Furthermore, it has been shown that the auxin-response transcription factor AUXIN RESPONSE FACTOR 7 (ARF7) is sumoylated in cells on the air side of roots, promoting binding to the repressor protein INDOLE-3-ACETIC ACID INDUCIBLE 3 (IAA3), which blocks the initiation of lateral root founder cells (*18*). To identify

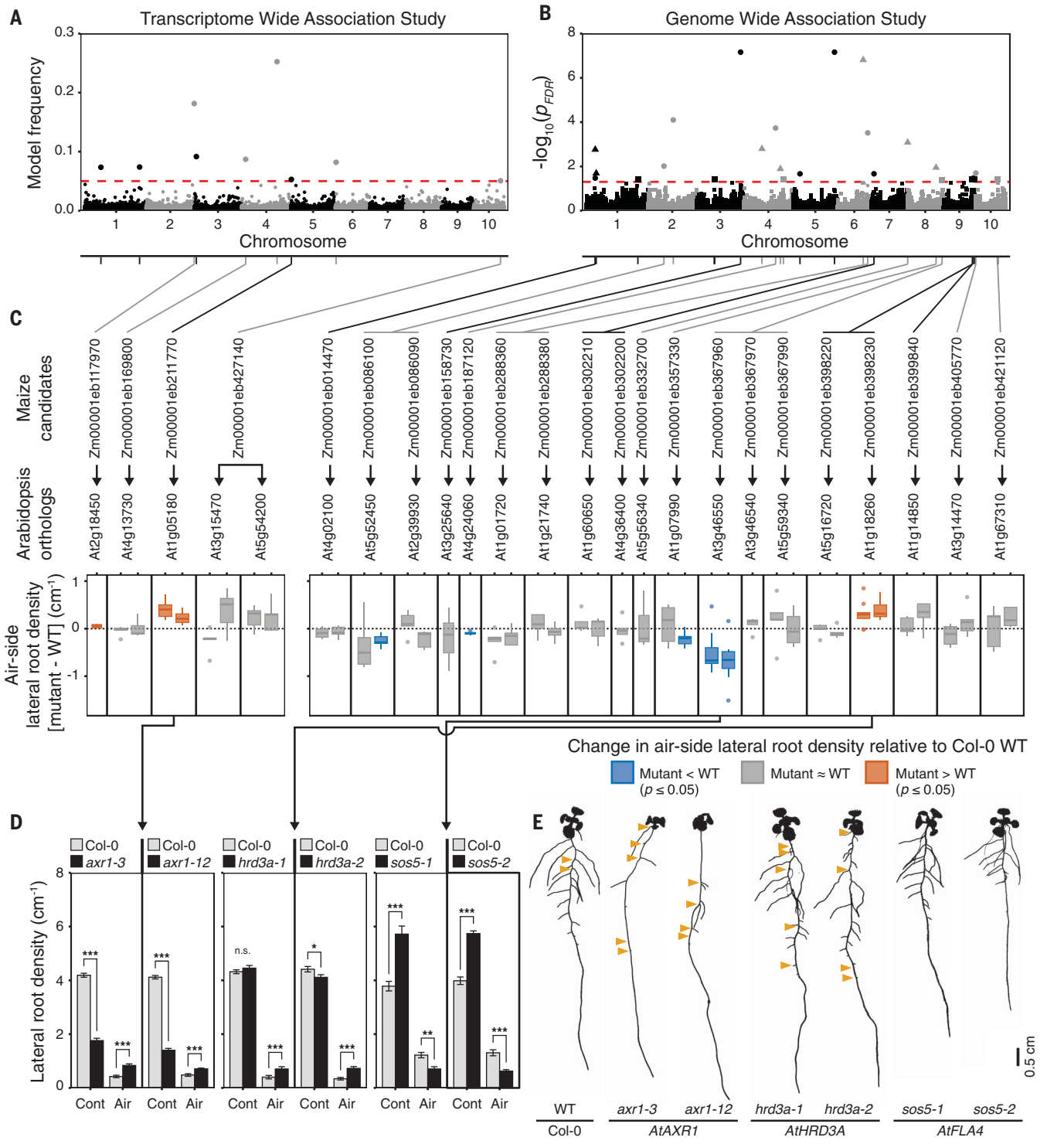

Fig. 3. Genetic control for hydropatterning revealed in maize and validated in *Arabidopsis*. (**A** and **B**) Manhattan plots of TWASs and GWASs for air-side lateral root density in maize. (A) TWAS used gene expression data from maize root tips (*19*). Significance threshold: model frequency = 0.05 (red dashed line). (B) GWAS shows smallest value for each SNP across three minor allele frequency cutoffs: ≥0.4% (solid circles), ≥2.2% (solid triangles), and ≥4.4% (solid squares). $P = 0.05$, FDR-adjusted significance threshold (red dashed line). Gray and black lines connect SNPs and associated candidate genes corresponding to the chromosome coloration. (**C**) Validation of maize candidate genes using mutants of corresponding gene orthologs in *Arabidopsis*. Air-side lateral root densities of mutants are shown relative to Col-0 WT. Fill color denotes significant differences ($P \leq 0.05$, paired Student's *t* test): mutants > WT are shown in orange, mutants < WT in blue, and not significant in gray; $n = 5$ to 10 plates per mutant (five WT and five mutant seedlings per plate). (**D**) Comparisons of contact-side (Cont) and air-side (Air) lateral root densities between Col-0 WT (gray) and mutants for *AtAXR1*, *AtHRD3A*, and *AtFLA4* (all mutants black). $n = 10$ plates per mutant (five WT and five mutant seedlings per plate). Asterisks denote significant differences (*$P \leq 0.05$, **$P \leq 0.01$, ***$P \leq 0.001$, paired Student's *t* test). Bar graphs indicate the mean ± SEM. (**E**) Binary images of 11-d-old seedlings. Orange triangles mark air-side lateral roots. Scale bar, 0.5 cm. Dilation was used on images to improve visibility.

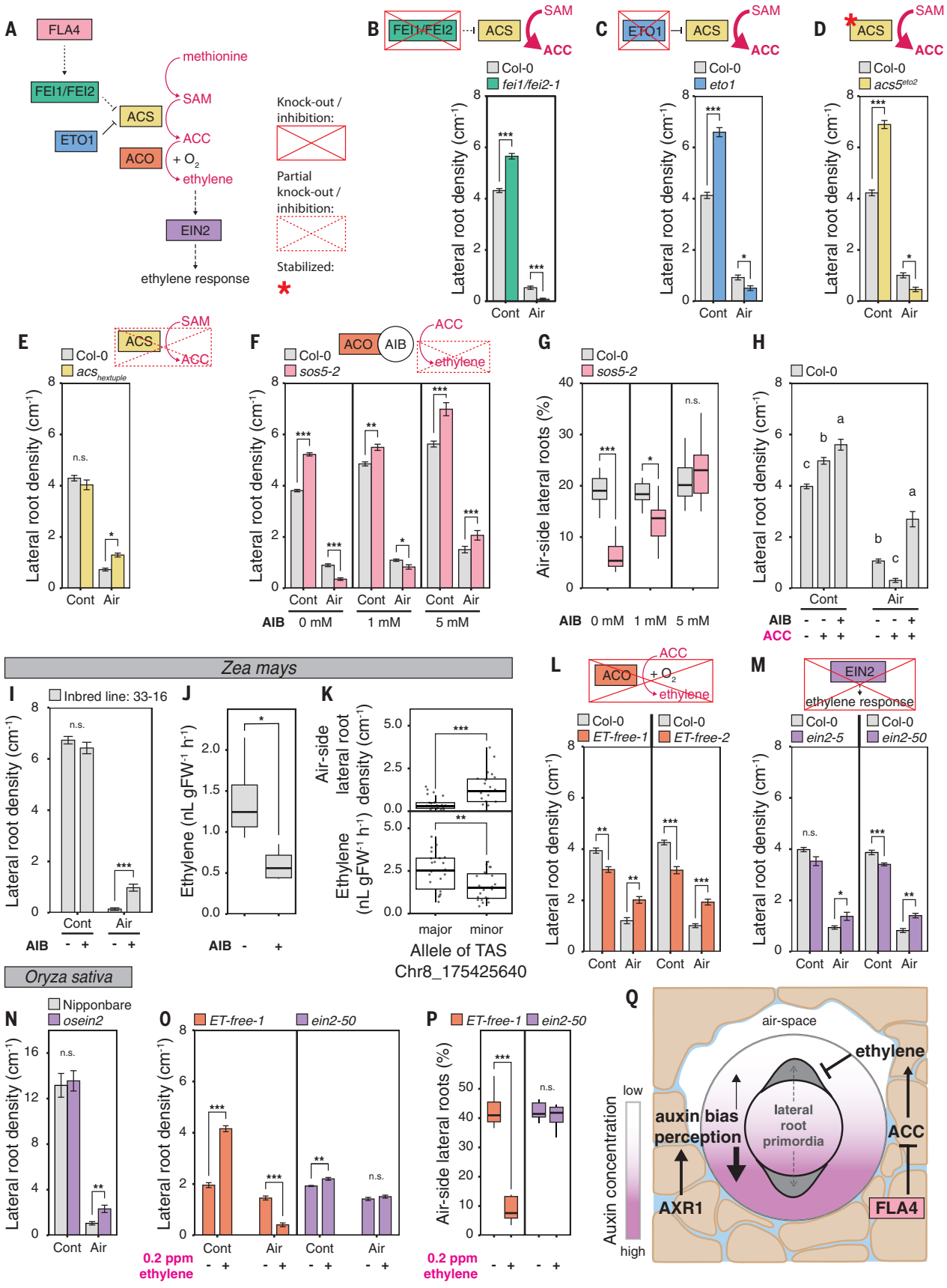

Fig. 4. Ethylene inhibits the formation of air-side lateral roots in *Arabidopsis*, maize, and rice. (**A**) FLA4 and the ethylene pathway in *Arabidopsis* (*27*). (**B** to **E**) Contact-side (Cont) and air-side (Air) lateral root densities in *Arabidopsis* mutants *eto1* (blue, *n* = 5 plates) (C), $acs5^{eto2}$ (yellow,

n = 5 plates) (D), and *acs2-1/4-1/5-2/6-1/7-1/9-1* hextuple mutant (yellow, *n* = 5 plates) relative to Col-0 (gray) (E). (**F** and **G**) Effect of AIB on *Arabidopsis* mutant *sos5-2* relative to Col-0 (pink, *n* = 10 plates per treatment). (**H**) *Arabidopsis* Col-0 response to ACC, AIB, and combination: − indicates mock control and + indicates plus 0.05 mM ACC or 5 mM AIB; *n* = 10 plates per treatment. Letters denote significant differences between treatments (ANOVA, post-hoc Tukey HSD test). (**I** and **J**) Response of maize inbred 33-16 to (+) 10 mM AIB relative to (−) mock control (*n* = 20 plants per treatment), and related ethylene production (*n* = 4 samples of five roots per treatment). (**K**) Air-side lateral root density and root ethylene production for maize inbred lines (*n* = 22/allele) with the major (G) or minor (T) allele at TAS Chr8_175425640. (**L** to **N**) Contact- and air-side lateral root densities in *Arabidopsis* mutants *ET-free-1* and *ET-free-2* (orange, *n* = 8 to 9 plates) (L) and *ein2-5* and *ein2-50* (purple, *n* = 10 plates) relative to Col-0 (M), and in rice mutant *osein2* (purple, *n* = 11 seedlings) relative to Nipponbare WT (gray, *n* = 16 seedlings) (N). (**O** and **P**) Effect of exogenous ethylene treatment on *Arabidopsis* mutants *ET-free-1* (*n* = 8 plates per treatment) and *ein2-50* (*n* = 8 plates per treatment). (**Q**) Working model of hydropatterning controlled by auxin and ethylene. Asterisks denote significant differences (*$P \leq 0.05$, **$P \leq 0.01$, ***$P \leq 0.001$, Student's *t* test), n.s., not significant. Bar graphs indicate mean ± SEM.

new loci and associated genes for hydropatterning with relevance to maize, we conducted genome-wide (GWAS) and transcriptome-wide (TWAS) association studies, which associate single-nucleotide polymorphisms (SNPs) or variations in gene expression among the study population with variation in a trait of interest.

TWAS (*13*) identified nine genes with expression in germinating seedling roots (*19*) that was significantly associated with differences in air-side lateral root density (Fig. 3A and data S7). Among these TWAS genes, we found *Zm00001eb211770*, a maize ortholog of *AUXIN RESISTANT 1* (*ZmAXR1*). In *Arabidopsis*, AXR1 together with E1 C-terminal related 1 (ECR1) act as ubiquitin-activating enzymes that facilitate the RUB modification of CULLIN 1 (CUL1), which is part of the $SCF^{TIR/AFB}$ complex at the center of auxin perception. RUB modification is necessary to allow auxin signal transduction for lateral root induction (*20*). TWAS in maize found that higher gene expression of *ZmAXR1* is associated with increased air-side lateral root densities (fig. S6A and data S7), which may be due to an increased sensitivity for auxin perception, leading to more frequent induction of lateral roots on the air side. To analyze the origin of the variation in *ZmAXR1* gene expression, we mapped the associated expression quantitative trait loci. This analysis revealed several significant expression-associated SNPs (e-SNPs) (fig. S6B and data S8 and S9). The most significant e-SNP, Chr5_2705946, colocalized with *ZmAXR1* itself, indicating that cis-acting regulatory variation may explain the variation in *ZmAXR1* gene expression associated with air-side lateral root density. Input data for the TWAS suggested expression of *ZmAXR1* in root tips of most inbred lines (fig. S6A). This was confirmed through in situ detection of *ZmAXR1* transcripts in root tips of the maize inbred line B73 by hybridization chain reaction (fig. S7, A to C). These results indicate that auxin regulation and related processes play a role in hydropatterning for maize roots, as previously demonstrated in *Arabidopsis* (*5*, *18*).

In parallel, GWAS (*21*, *22*) identified 30 unique trait-associated SNPs (TASs) for air-side lateral root density (Fig. 3B; fig. S6, C and D; and data S10), suggesting that variation in hydropatterning is controlled by numerous loci in maize. In almost all cases, higher air-side lateral root density was associated with the less-frequent allele (minor allele) of the TAS within our population, except for TAS Chr8_143668219, as shown by the effect estimate (data S10). This supports our hypothesis that weakening of hydropatterning may have been caused by relaxation of selection, because selection typically constrains the occurrence of genetic variants (*23*). We identified a total of 40 genes within 20-kb windows centered on the TASs. In cases where no gene was located within these windows, the next closest gene was included (data S11). These were considered candidates for genes that may control air-side lateral root density in maize.

Validation of maize candidate genes using *Arabidopsis* orthologs

We identified maize candidate gene orthologs in *Arabidopsis* and screened available mutant lines for hydropatterning defects (fig. S8A and data S12 and S13). Screening revealed seven genes for which at least one mutant allele showed a significant change in air-side lateral root density and percentage of air-side lateral roots (Fig. 3C and fig. S8B). For three of these genes, two independent mutant alleles both showed significant, matching changes in air-side lateral root density, confirming their association with hydropatterning (Fig. 3, D and E)

The auxin-signaling pathway mutants *axr1-3* and *axr1-12* of *AtAXR1* showed significant increases in air-side lateral root density and percentage of air-side lateral roots compared with the wild type (WT), whereas contact-side lateral root density decreased significantly (Fig. 3, D and E). This defect is similar to the phenotype of other auxin-pathway mutants in *Arabidopsis* (*5*, *18*), and it confirms that the auxin hormone pathway plays an important role in promoting the bias in lateral root development toward the moisture-contacting side of the root both in *Arabidopsis* and maize.

Similarly, we observed significant increases in air-side lateral root density and percentage of air-side lateral roots in *Arabidopsis* mutants of HMG-CoA REDUCTASE DEGRADATION 3A (*AtHRD3A*), *hrd3a-1* and *hrd3a-2* (Fig. 3, D and E). *AtHRD3A*, an ortholog of GWAS candidate *Zm00001eb398230* (*ZmHRD3A*), recruits misfolded proteins for endoplasmic reticulum–associated protein degradation to the HRD1/HRD3 complex (*24*). Targets include misfolded receptor-like kinases and glycosylated proteins (*25*), suggesting that hydropatterning may rely upon proteins acting at the plasma membrane that are also targets of endoplasmic reticulum–associated protein degradation. In contrast to mutants of *AtAXR1*, *hrd3a-1* and *hrd3a-2* showed either no changes or a relatively small change in contact-side lateral root densities, respectively. This suggests that HRD3A may primarily function in the suppression of air-side lateral root development. In maize, *ZmHRD3A* was discovered as one of three candidate genes associated with TAS Chr9_147576641 (data S11). Mutants of *At5g16720*, an ortholog of *Zm00001eb398220* associated with the same TAS, did not affect hydropatterning (fig. S8B). *ZmHRD3A* is expressed at the root tip in the same region where moisture signals control the patterning of lateral roots (fig. S7, A and D).

In contrast to *axr1* and *hrd3a*, *Arabidopsis* mutants of *FASCICLIN-LIKE ARABINOGALACTAN-PROTEIN 4* (*AtFLA4*), named *salt overly sensitive5* (*sos5-1* and *sos5-2*), showed significant strengthening of hydropatterning with decreases in air-side lateral root density and percentage of air-side lateral roots compared with WT (Fig. 3D). The mutant *sos5-1* was identified for its defects in growth on saline media (*26*). Although the primary root phenotype under salinity and ionic stress has been studied extensively (*27*), no reports have described a lateral root phenotype. *AtFLA4* belongs to a group of 21 fasciclin-like arabinogalactan proteins and carries two fasciclin 1 domains that allow it to interact with the extracellular cell wall matrix (*28*, *29*), which may allow it to sense extracellular cues originating from the environment. The decrease in air-side lateral root density in the *sos5* mutants was accompanied by a significant increase in contact-side lateral root density and a significant reduction in primary root length (Fig. 3, D and E, and fig. S9A). Taking this reduction of primary root length into account, *sos5-1* and *sos5-2* both showed a significant decrease in the total number of emerged air-side lateral roots per seedling, but only a small or no increase in total contact-side lateral roots per seedling (fig. S9B). Thus, these data indicate that *sos5* primarily suppresses air-side lateral roots, whereas changes in contact-side lateral root density may result from pleiotropic effects on root length. *AtFLA4* is an ortholog of GWAS candidate *Zm00001eb367960*

(*ZmFLA4*), which was discovered as one of four candidate genes associated with TAS Chr8_175425640 (data S11). Similar to *AtFLA4*, *ZmFLA4* contains two fasciclin 1 domains (*30*). Orthologous *Arabidopsis* mutants of two other candidate genes associated with the same TAS, *Zm00001eb367970* and *Zm00001eb367990*, showed no defect in hydropatterning (fig. S8B). This provides evidence that variation associated with *ZmFLA4* may be the primary determinant of the observed variation in hydropatterning at TAS Chr8_175425640. In maize, *ZmFLA4* is expressed at the root tip (fig. S8, A and E).

Ethylene as an air-side signal mediating hydropatterning

Ethylene is a gaseous plant hormone that regulates development in response to several abiotic stresses (*31*). Accumulation of root-produced ethylene in compacted soils serves as a signal leading to root growth inhibition (*32*). In *Arabidopsis*, *AtFLA4* may act in a genetic pathway regulating the synthesis of ethylene precursor 1-aminocyclopropane-1-carboxylate (ACC) from S-adenosylmethionine (SAM) (Fig. 4A) (*27*). In this pathway, AtFLA4 acts upstream of two leucine-rich repeat receptor-like kinases, AtFEI1 and AtFEI2 (*33*). These kinases interact with 1-AMINOCYCLOPROPANE-1-CARBOXYLATE SYNTHASE (ACS) 5 and 9, which are involved in the synthesis of ACC. Associated with this pathway, ETHYLENE OVERPRODUCER 1 (AtETO1) functions as a negative regulator of type-2 ACS enzymes, including ACS5 and ACS9 (*34*).

We found that double mutants of *AtFEI1* and *AtFEI2* (*fei1*/*fei2-1*), as well as single mutants of *AtETO1* (*eto1*) and *AtACS5* ($acs5^{eto2}$, which carries a C-terminal mutation in ACS5 that increases protein stability), all showed similar reductions in air-side lateral root density as observed in the *AtFLA4* mutants *sos5-1* and *sos5-2*. Concomitantly, all mutants showed an increase in contact-side lateral root density and a reduction in primary root length (Fig. 4, B to D, and fig. S9, C to E). Screening of the single mutants *fei1* and *fei2-1* revealed no significant effects on air-side lateral root density (fig. S9F), corroborating a suggestion that both genes may act in a redundant fashion (*33*). Although both *eto1* and $acs5^{eto2}$ increase ACC synthesis, a reduction of ACC synthesis in the *AtACS* hextuple mutant (*acs2-1*, *acs4-1*, *acs5-2*, *acs6-1*, *acs7-1*, and *acs9-1*) led to a significant increase in air-side lateral root density (Fig. 4E). We also tested the single mutant *acs5-1*, but observed no difference compared with WT (fig. S9G). This result is likely due to the high level of redundancy between *ACS* genes in *Arabidopsis*, which has eight functional ACS homologs (*35*). Our results suggest that genetic modulation of ACC synthesis affects hydropatterning in a way that resembles the phenotypes of *sos5-1* and *sos5-2*.

Next, we investigated whether ACC itself or ethylene, which is synthesized from ACC by ACC-oxidases (ACOs), causes the observed repression in air-side lateral root development. We found that treatment with 2-aminoisobutyric acid (AIB), a competitive inhibitor of ACOs, caused an increase in air-side lateral root density and rescued the *sos5-2* mutant phenotype (Fig. 4, F and G). Likewise, treatment of Col-0 WT with ACC alone reduced air-side lateral root density, likely due to the increased production of ethylene, because this effect was reversed by cotreatment with AIB (Fig. 4H). Both ACC and ACC + AIB treatments showed significant increases in contact-side lateral root density compared with mock-treated Col-0 WT. These increases could be due to a concomitant reduction in primary root length with both treatments (fig. S9H) and/or to the effects of ACC itself on lateral root induction (*36*). Taken together, these observations suggest a central role for ethylene in the suppression of air-side lateral root development that does not require localized ACC synthesis, because exogenous ACC application on the contact side was able to induce the same effect.

In maize, AIB treatment of a strong hydropatterning inbred line 33-16 increased air-side lateral root density and significantly reduced ethylene production (Fig. 4, I and J). This indicates that ethylene suppresses air-side lateral root development in maize as well. Measurements of ethylene production from root tips of maize inbred lines that either carry the major or minor allele for TAS Chr8_175425640, localized ~2 kb upstream of *ZmFLA4*, showed that the minor allele was associated with lower ethylene production and higher air-side lateral root densities (Fig. 4K). This may suggest that TAS Chr8_175425640 is linked to genetic variation that affects *ZmFLA4* function, leading to the observed differences in ethylene production.

Complete disruption of ethylene synthesis in two *AtACO* quintuple mutants (*ET-free-1* and *ET-free-2*), in which all five *AtACO* genes were mutated by CRISPR/Cas9 (*37*), showed a significant increase in air-side lateral root density (Fig. 4L). Similarly, the ethylene perception mutants *ein2-5* and *ein2-50* showed a significant increase in air-side lateral root density (Fig. 4M). These observations confirm that ethylene suppresses air-side lateral root development. Concomitantly, we observed a decrease in contact-side lateral root density for *ET-free-1*, *ET-free-2*, *ein2-5*, and *ein2-50* that mirrored the increase in air-side lateral root density leading to no change in total lateral root density (fig. S9, I and J). Because lateral root induction can only occur at one of the two xylem poles in *Arabidopsis* (*38*), it is possible that a derepression of air-side lateral root development in these mutants leads to lateral root redistribution from the contact side. Although mutants for *EIN2* have not been described in maize, a mutant allele of *OsEIN2* in rice was available and showed a similar defect in hydropatterning as the *Arabidopsis* mutant alleles (Fig. 4N), providing further evidence that ethylene-dependent regulation of hydropatterning is conserved between *Arabidopsis* and grasses. A double mutant of ETHYLENE-INSENSITIVE3 (EIN3) and ETHYLENE-INSENSITIVE3-LIKE 1 (EIL1), *ein3/eil1*, two major transcriptional regulators of ethylene signaling that act downstream of EIN2, showed no difference in air-side lateral root density compared with Col-0 WT (fig. S9K). This might be due to redundancy in transcriptional regulation or to an alternative pathway (*39*) that leads to air-side suppression of lateral root development by ethylene. Exogenous treatment of *ET-free-1* and *ein2-50* with 0.2 ppm ethylene was sufficient to suppress air-side lateral root development in *ET-free-1*, whereas *ein2-50* showed no response (Fig. 4, O and P). Our results suggest that localized ethylene synthesis is not necessary, and additional mechanisms must exist that control air-side specific suppression of lateral roots by ethylene.

Because auxin is necessary for lateral root induction and ethylene has been shown to induce local auxin biosynthesis (*40*), we generated a double mutant of *sos5-2* and *axr1-3* to study their epistatic interactions. Although the disruption of auxin signaling led to an increase in air-side lateral roots, the double mutant *sos5-2*/*axr1-3* showed a significant decrease in air-side lateral root density (fig. S9L). Our results indicate an additive interaction between auxin and ethylene responses. Further work will be necessary to elucidate how air-side lateral root suppression by ethylene is connected to auxin-controlled lateral root induction on the contact side.

Conclusions

Our results reveal that hydropatterning is a crop-relevant response of roots to heterogeneity in soil moisture. The development of modern breeding germplasm in maize led to the weakening of hydropatterning in temperate regions, likely through relaxation of selection. This divergence in hydropatterning may relate to the different selection pressures experienced by each subpopulation. Using genetic analyses, we detected associations between hydropatterning and the auxin- and ethylene-signaling pathways. Investigation of these pathways in maize, rice, and *Arabidopsis* demonstrated that auxin signaling promotes a bias in lateral root development toward moisture-contacting surfaces of the root, whereas ethylene suppresses branching on air-exposed surfaces (Fig. 4Q and fig. S9M). FLA4, acting at the top of a signaling pathway that restricts ethylene biosynthesis, may perceive an as-yet-unknown environmental cue to tune the degree to which root architecture is responsive to local soil structure and water availability. Further genetic work in maize is needed to validate our findings in *Arabidopsis*.

A deeper understanding of these pathways may allow for the control of moisture-responsive root growth to improve drought resilience in maize.

REFERENCES AND NOTES

1. Y. Satoh *et al*., *Nat. Commun.* **13**, 3287 (2022).
2. J. P. Lynch, *Plant J.* **109**, 415–431 (2022).
3. M. C. Drew, *New Phytol.* **75**, 479–490 (1975).
4. P. Voothuluru, Y. Wu, R. E. Sharp, *Plant Cell* **36**, 1377–1409 (2024).
5. Y. Bao *et al*., *Proc. Natl. Acad. Sci. USA.* **111**, 9319–9324 (2014).
6. J. D. Scharwies, J. R. Dinneny, *J. Plant Res.* **132**, 311–324 (2019).
7. J. R. Dinneny, *Annu. Rev. Cell Dev. Biol.* **35**, 239–257 (2019).
8. S. A. Flint-Garcia *et al*., *Plant J.* **44**, 1054–1064 (2005).
9. N. E. Robbins II, J. R. Dinneny, *Proc. Natl. Acad. Sci. USA.* **115**, E822–E831 (2018).
10. L. Jansen, I. Roberts, R. De Rycke, T. Beeckman, *Philos. Trans. R. Soc. Lond. B Biol. Sci.* **367**, 1525–1533 (2012).
11. R. V. Mural *et al*., *Gigascience* **11**, giac080 (2022).
12. Z. Zheng *et al*., *Plant Physiol.* **182**, 977–991 (2020).
13. H.-Y. Lin *et al*., *Genome Biol.* **18**, 192 (2017).
14. A. Zhan, H. Schneider, J. P. Lynch, *Plant Physiol.* **168**, 1603–1615 (2015).
15. Y. Wu *et al*., *Theor. Appl. Genet.* **129**, 753–765 (2016).
16. S. K. Vasal, S. Mclean, *The Lowland Tropical Maize Subprogram* (CIMMYT, 1994).
17. A. W. Santure, J. Wang, *Genetics* **181**, 259–276 (2009).
18. B. Orosa-Puente *et al*., *Science* **362**, 1407–1410 (2018).
19. K. A. G. Kremling *et al*., *Nature* **555**, 520–523 (2018).
20. J. C. del Pozo *et al*., *Plant Cell* **14**, 421–433 (2002).
21. X. Liu, M. Huang, B. Fan, E. S. Buckler, Z. Zhang, *PLOS Genet.* **12**, e1005767 (2016).
22. A. Kusmec, P. S. Schnable, *Plant Direct* **2**, e00053 (2018).
23. M. Lynch *et al*., *Nat. Rev. Genet.* **17**, 704–714 (2016).
24. W. Su, Y. Liu, Y. Xia, Z. Hong, J. Li, *Proc. Natl. Acad. Sci. USA.* **108**, 870–875 (2011).
25. S. Hüttner, R. Strasser, *Front. Plant Sci.* **3**, 67 (2012).
26. H. Shi, Y. Kim, Y. Guo, B. Stevenson, J.-K. Zhu, *Plant Cell* **15**, 19–32 (2003).
27. G. J. Seifert, *Genes* **12**, 145 (2021).
28. K. L. Johnson, B. J. Jones, A. Bacic, C. J. Schultz, *Plant Physiol.* **133**, 1911–1925 (2003).
29. H. Xue *et al*., *Plant J.* **91**, 613–630 (2017).
30. C. J. A. Sigrist *et al*., *Brief. Bioinform.* **3**, 265–274 (2002).
31. H. Chen, D. A. Bullock Jr., J. M. Alonso, A. N. Stepanova, *Plants* **11**, 33 (2021).
32. B. K. Pandey *et al*., *Science* **371**, 276–280 (2021).
33. S.-L. Xu, A. Rahman, T. I. Baskin, J. J. Kieber, *Plant Cell* **20**, 3065–3079 (2008).
34. H. Yoshida, M. Nagata, K. Saito, K. L. C. Wang, J. R. Ecker, *BMC Plant Biol.* **5**, 14 (2005).
35. A. Tsuchisaka *et al*., *Genetics* **183**, 979–1003 (2009).
36. J. K. Polko, J. J. Kieber, *Front. Plant Sci.* **10**, 1602 (2019).
37. W. Li *et al*., *Mol. Plant* **15**, 354–362 (2022).
38. B. Parizot *et al*., *Plant Physiol.* **146**, 140–148 (2008).
39. B. M. Binder, L. A. Mortimore, A. N. Stepanova, J. R. Ecker, A. B. Bleecker, *Plant Physiol.* **136**, 2921–2927 (2004).
40. A. N. Stepanova *et al*., *Cell* **133**, 177–191 (2008).
41. J. D. Scharwies *et al*., Data for: Moisture-responsive root-branching pathways identified in diverse maize breeding germplasm, Zenodo (2024); https://doi.org/10.5281/zenodo.13347148.
42. J. D. Scharwies *et al*., Data for: Moisture-responsive root-branching pathways identified in diverse maize breeding germplasm, Dryad (2024); https://doi.org/10.5061/dryad.3ffbg79sv.

ACKNOWLEDGMENTS

We gratefully acknowledge the many thoughtful discussions with V. Walbot (Stanford University) regarding experiments in maize. We also thank the USDA-ARS US National Plant Germplasm System for providing the maize seeds from the Goodman-Buckler association panel; S. Leiboff (Oregon State University) and C. Rasmussen (University of California–Riverside) for providing the maize DII-VENUS-NLS reporter lines; C. Schultz (University of Adelaide) and G. Seifert (BOKU Vienna) for discussions regarding the function and role of FLA4; staff at Stanford University and the Carnegie Institution for Science for their support; and all members of the Dinneny laboratory for their help with revisions of the draft manuscript. **Funding:** This work was supported by a Faculty Scholars Grant from the Simons Foundation and Howard Hughes Medical Institute (grant 55108515 to J.R.D.); the Advanced Research Projects Agency-Energy (ARPA-E), US Department of Energy (DE-AR grant 1565-1555 to J.R.D. and DE-AR grant 0000826 to P.S.S.); the Biological and Environmental Research (BER) Program, US Department of Energy (grant DE-SC0023160 to J.R.D.); a Howard Hughes Medical Institute Investigator award (J.R.D.); the National Science Foundation (grant MCB-2427432 to J.K.); UKRI Frontiers Research ERC StG (grant EP/Y036697/1 to B.K.P.); the Biotechnology and Biological Sciences Research Council (BBSRC) (grant BB/V003534/1 to C.J.S., J.B., and M.B. and grants BB/T001437/1, BB/W008874/1, and BB/W015080/1 to M.B.); the European Research Council (grant HYDROSENSING 101118769 to M.B.); HORIZON EUROPE (Marie Sklodowska-Curie Actions grant 765000 to M.A.V.); and EVOTREE (grant RCN 287465 to S.B.). **Author contributions:** Conceptualization: J.D.S., J.R.D.; Data acquisition: J.D.S., T.C., A.D., C.J.S., J.B., H.H.T.-M., W.G.V.; Data analysis: J.D.S., Z.Z., S.B., M.A.V.; Funding acquisition: J.R.D., J.K., B.K.P., P.S.S., C.J.S., J.B., M.B., M.A.V., S.B.; Project administration: J.D.S.; Resources: R.K., J.K., B.K.P., M.B., P.S.S.; Supervision: J.D.S., J.R.D.; Visualization: J.D.S., C.J.S., S.B., M.A.V.; Writing – original draft: J.D.S., J.R.D.; Writing – review & editing: all authors. **Competing interests:** P.S.S. is a cofounder and CEO of Dryland Genetics, Inc.; a cofounder and managing partner of Data2Bio, LLC; a member of the scientific advisory boards of Kemin Industries and Centro de Tecnologia Canavieira; and the recipient of research funding from Iowa Corn and Bayer Crop Science. The remaining authors declare no competing interests. **Data and materials availability:** Data and summary statistics are available in the supplementary materials. Software, raw data, and code for image processing to generate data, statistics, and figures are available on Dryad and Zenodo (*41*, *42*).

SUPPLEMENTARY MATERIALS

science.org/doi/10.1126/science.ads5999
Materials and Methods
Figs. S1 to S9
References (*43*–*72*)
Data S1 to S16
MDAR Reproducibility Checklist

Submitted 21 August 2024; accepted 6 January 2025
10.1126/science.ads5999